NANO LETTERS

2002
Vol. 2, No. 8
869−872

High Performance Electrolyte Gated Carbon Nanotube Transistors

Sami Rosenblatt,[†] Yuval Yaish,[†] Jiwoong Park,[†,‡] Jeff Gore,[‡] Vera Sazonova,[†] and Paul L. McEuen*[,†]

Laboratory of Atomic and Solid State Physics, Cornell University, Ithaca, New York 14853 and Department of Physics, University of California, Berkeley, California 94720

Received June 7, 2002

ABSTRACT

We have fabricated high performance field-effect transistors made from semiconducting single-walled carbon nanotubes (SWNTs). Using chemical vapor deposition to grow the tubes, annealing to improve the contacts, and an electrolyte as a gate, we obtain very high device mobilities and transconductances. These measurements demonstrate that SWNTs are attractive for both electronic applications and for chemical and biological sensing.

Field effect transistors (FETs) made from semiconducting single-walled carbon nanotubes (SWNTs) have been intensely investigated[1−6] since they were first made in 1998.[7] The reported properties of SWNT transistors have varied widely due to variations in the quality of the nanotube material, the device geometry, and the contacts. Optimizing their properties is crucial for applications in both electronics and in chemical and biological sensing. For electronic applications, a number of parameters dictate the performance of an FET, such as mobility and transconductance. For sensing,[8,9] the ability to work in the appropriate environment (e.g., salty water for biological applications) is critical. Here we report on optimized SWNT transistors where an electrolyte solution is used as a gate. The high mobilities, low contact resistances, and excellent gate coupling of these devices yield device characteristics that significantly exceed previous reports. They show that SWNT transistors are very attractive for both electronics and molecular sensing.

The nanotube (NT) devices were prepared following an approach similar to that of Kong et al.[10] A completed device is shown in Figure 1a and b. Catalyst islands containing $Fe(NO_3)_3 \cdot 9H_2O$, $MoO_2(acac)_2$, and alumina nanoparticles were defined on a 200 nm thick thermally grown oxide over a degenerately doped Si substrate that can be used as a back gate. Photolithography and etching were then used to pattern a poly(methyl methacrylate) (PMMA) layer, which was subsequently used as a lift-off mask for the catalyst. NTs were then grown by chemical vapor deposition. Metal electrodes consisting of Cr (5 nm) and Au (50 nm) were then patterned over the catalyst islands using photolithography and a lift-off process, with a spacing between source and drain electrodes between 1 and 3 microns. The tube diameters were determined from atomic force microscope measurements such as the one in Figure 1b. An anneal at 600 °C for 45 min in an argon environment was used to improve the contact resistance between the tubes and the electrodes (typically by an order of magnitude).

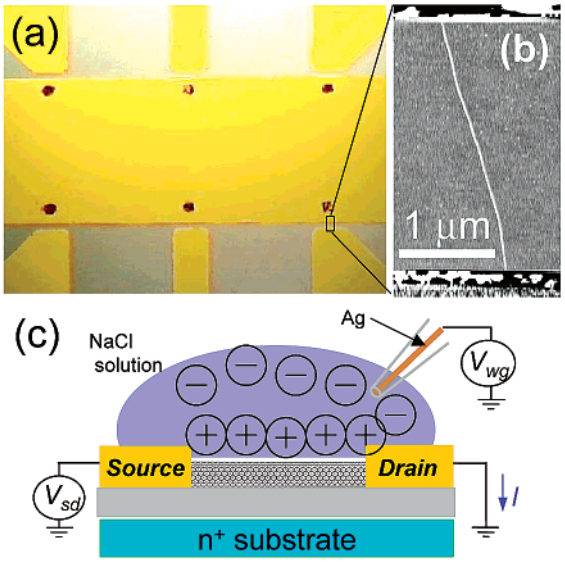

Figure 1. (a) Optical micrograph of the device. Six catalyst pads (dark) can be seen inside area of the common electrode. Correspondingly, there are six source electrodes for electrical connection to tubes. (b) AFM image of a tube between two electrodes. The tube diameter is 1.9 nm. (c) Schematic of the electrolyte gate measurement. A water gate voltage V_{wg} is applied to droplet through a silver wire.

* Corresponding author.
[†] Cornell University.
[‡] University of California, Berkeley.

10.1021/nl025639a CCC: $22.00
Published on Web 07/25/2002

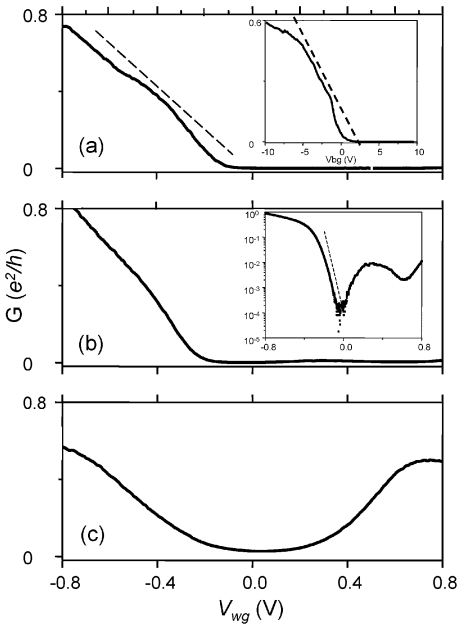

Figure 2. Conductance G versus water gate voltage V_{wg} for three tubes with lengths and diameters given by: (a) $L = 1\ \mu$m, $d = 1.1$ nm, (b) $L = 1.4\ \mu$m, $d = 3$ nm, and (c) $L = 2.2\ \mu$m, $d = 4.3$ nm wide. Inset to (a): G versus the back gate voltage V_{bg} for the same device measured in vacuum; the slope of linear regime is given by dashed line. Inset to (b): Logarithmic scale plot showing the exponential dependence of G on V_{wg} for the same device.

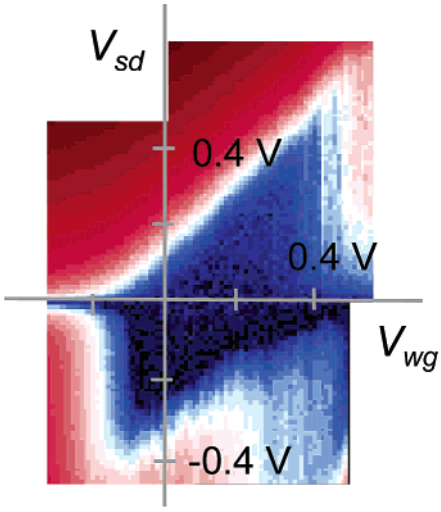

Figure 3. Grayscale plot of current on a logarithmic scale versus V_{wg} and V_{sd} for the device of Figure 2b. The band gap region is given by the dark trapezoid at the center.

In the experiments reported here, we measure the conductance through the tube using an electrolyte as a gate, as schematically shown in Figure 1c. This approach was first used by Krüger et al.[11] to study multiwalled NTs. A micropipet is used to place a small (∼10−20 micron diameter) water droplet over the nanotube device. A voltage V_{wg} applied to a silver wire in the pipet is used to establish the electrochemical potential in the electrolyte relative to the device. For $-0.9\text{V} < V_{wg} < 0.9$ V, the leakage current between the water and the Au electrodes/SWNT was negligible (less than 1 nA); the electrolyte then functions as a well-insulated liquid gate. Above this range, the electrolyte reacts with the Au electrodes and destroys the device.

The main panels of Figure 2 show the low-bias conductance G vs V_{wg} for three nanotubes with increasing diameters, where the electrolyte is 10 mM NaCl. The conductance is large at negative V_{wg}, corresponding to p-type conduction in the tube, decreasing approximately linearly to zero. It remains near zero for a range near 0 V, and then increases again at positive V_{wg}. This corresponds to n-type transport. In the n-type region, the conductance is significantly less than in the p-type region, particularly for smaller diameter SWNTs. Figure 3 shows a grayscale plot of the current of the device shown in Figure 2b as a function of both V_{sd} and V_{wg}. The low conductance region corresponding to the band gap of the tube is clearly seen, with p- and n-type conductance observed at negative and positive V_{wg}, respectively. The low-conductance region is trapezoidal in shape, with the boundaries given by a line with slope $dV_{sd}/dV_{wg} \cong 1$. The device conductance diminishes exponentially in the subthreshold (gap) region as is seen in the inset to Figure 2b. The slope of the exponential falloff gives a device parameter known as the subthreshold swing $S = -[d(\log G)/dV_{wg}]^{-1}$, which is ∼80 mV/decade for this device. Other devices give similar values.

Theoretically, the exponential falloff corresponds to thermal activation of carriers in the semiconductor: $G \sim \exp(-E_b/kT)$ where E_b is the energy from the Fermi level to the nearest of the conduction and valence bands. This barrier height changes linearly with V_{wg}: $\delta E_b = e\alpha\delta V_{wg}$, where α is a numerical constant that measures the effectiveness with which the gate modulates the band energies. The theoretical upper limit $\alpha = 1$ gives $S = 60$ mV/decade. For the device in Figure 2b ($S = 80$ mV/decade), $\alpha = 0.75$; this is the highest value reported to date for SWNT transistors. The constant α can be used to infer the band gap of the tube of Figure 2b/Figure 3. From the measured width of the gap $\Delta V_{wg} \sim 0.45\ V$, we obtain $E_g = e\alpha\Delta V_{wg} \sim 0.33$ eV. This is in reasonable agreement with the expected value for a 3-nm tube obtained from the relation $E_g = 0.8\ eV/d$ [nm].[12]

Note that the size of the gap between n- and p-behavior decreases with increasing the diameter of the tube, as does the on-state conductance in n-type region compared to the p-region. This is evident from the traces of G vs V_{wg} in Figure 2. The suppression of n-type transport in small diameter tubes is consistent with previous measurements with back gated samples, where n-type transport was observable only in larger-diameter tubes[5,13] or in tubes whose contacts have been doped n-type.[14−17] This results from the fact that, under ambient conditions, Au contacts form p-type contacts to the tube. Depletion barriers thus form at the contacts in n-type operation, creating a large contact resistance to the tube. This barrier is larger the larger the band gap of the tube. As a result of these contact issues for n-type operation, we will concentrate our analysis on p-type operation.

The conductance change in the linear p-region for the device in Figure 2a is $dG/dV_{wg} \sim 1\ e^2/h/V$. Measurements from many other devices show similar behavior, with no obvious correlation between dG/dV_{wg} and the diameter of

the tube. Measurements were also done for salt concentrations varying between 0.1 mM to 100 mM; no strong dependence on the concentration was observed. For comparison, G versus back gate voltage V_{bg} applied to the substrate for the same device in operating in a vacuum is shown in the inset, yielding $dG/dV_{bg} \sim 0.08\ e^2/h/V$. The electrolyte gate is therefore ~10 times more effective in modulating the conductance of the tube than the back gate. The value dG/dV_{wg} is also an order of magnitude larger than values recently obtained using thin oxide back gates[4] and top gates.[6]

To quantitatively describe the transport in the p-region, we note that, in the incoherent limit, the total resistance of a SWNT with one subband occupied is the sum of three contributions, $R = h/4e^2 + R_c + R_t$. The term $h/4e^2$ is the quantized contact resistance expected for a 1D system with a 4-fold degenerate subband. In addition, imperfect contacts to the tube can give rise to an extra contact resistance R_c. Finally, the presence of scatters in the tube contribute a Drude-like conductance:

$$G_t = 1/R_t = C_g'|V_g - V_{go}|\mu/L$$

where C_g' is the capacitance per unit length of the tube, V_g is the gate voltage (back or electrolyte), V_{go} is the threshold gate voltage at which the device begins to conduct, and μ is the mobility. At low $|V_g - V_{go}|$, the device resistance is dominated by the intrinsic tube conductance G_t, which increases linearly with increasing V_g if μ is a constant. At large $|V_g - V_{go}|$, the device resistance saturates due to either the contact resistances or a V_g-independent tube resistance.

Using the equation for G_t given above, the mobility of carriers can be inferred if the capacitance per unit length of the SWNT is known. For the case of vacuum operation, the capacitance to the back gate C_{bg}' can be estimated from electrostatics[1] or inferred from Coulomb-blockade measurements,[18−20] yielding estimates from 1 to 3×10^{-11} F/m. Using a value $C_{bg}' = 2 \times 10^{-11}$ F/m, we obtain an inferred mobility $\mu \sim 1500$ cm^2/V−s for the vacuum data in Figure 2a. Figure 4 shows a histogram of the mobilities determined from a number of different samples operating in vacuum. Mobilities in the range of 1000 to 4000 cm^2/V−s are routinely obtained, with a few devices showing much higher values. Also shown is the maximum on-state conductance for the same samples. Values on the order of e^2/h are routinely obtained, within a factor of 4 of the theoretical limit of $4e^2/h$.

The high mobilities found here are comparable to the best reported to date for CVD-grown SWNTs,[3,21,22] and the maximum conductances are significantly better than previous reports. Both are significantly larger than the values found in devices using bulk-synthesized SWNT tubes and ropes.[1,2,4,6,17] The origin of this difference is not fully understood, but defects induced by ultrasonic/chemical processing of the tubes and/or disorder due to the presence of other tubes (in the case of ropes) may be responsible. The mobilities reported here are also significantly higher than those for holes in Si MOSFETs ($\mu < 500$ cm^2/V−s), indicating that SWNTs are remarkably high-quality semiconducting materials.

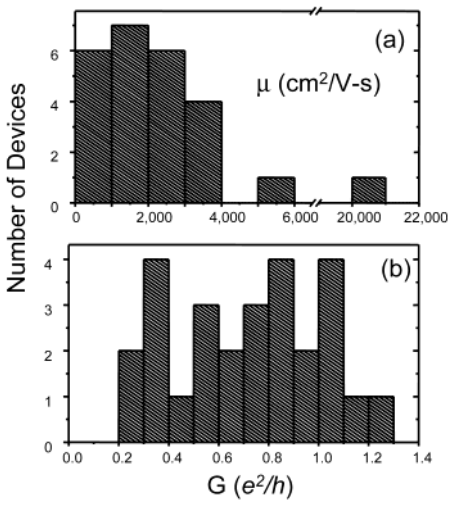

Figure 4. Histogram of (a) mobilities and (b) maximum conductances determined from measurements of individual SWNTs in vacuum.

For electrolyte gating, a simple estimate of the electrostatic capacitance between the tube and ions is given by $C_{ewg}' = 2\pi\epsilon\epsilon_o/\ln(1+2\lambda_D/d) \sim 7 \times 10^{-9}$ F/m for typical values of the dielectric constant and Debye screening length for salty water: $\epsilon = 80$ and $\lambda_D \sim 1$ nm. This value is more than 2 orders of magnitude larger than the back gate capacitance given above. There is an additional contribution to capacitance that is relevant in this case, however. The total capacitance, which relates the electrochemical potential difference applied between the tube and the gate to the charge on the tube, has both electrostatic and quantum (chemical) components: $1/C' = 1/C_e' + 1/C_Q'$, where C_e' is the electrostatic capacitance and $C_Q' = e^2 g(E)$, where $g(E)$ is the density of states for the SWNT. For a 1D tube, $g(E)$ is given by

$$g(E) = \frac{4}{\pi\hbar v_F}\frac{\sqrt{E^2 - (E_g/2)^2}}{E}$$

where $E > E_g/2$ is the energy of the electron measured relative to the center of the band gap. The quantum capacitance is therefore of order $C_Q' = 4e^2/\pi\hbar v_F = 4 \times 10^{-10}$ F/m for one subband occupied in the tube.

Note that it is the *smaller* of C_Q' and C_e' that dominates the overall capacitance C'. For the case of back gating, C_{ebg}' is nearly an order of magnitude smaller than C_Q', and therefore C_{ebg}' dominates. For water gating, on the other hand, C_Q' is an order of magnitude smaller than C_{ewg}' so C_Q' dominates. In principle, C_Q' goes to zero at the subband bottom, but thermal effects and the electrostatic capacitance C_e' will smear this out in the total capacitance C'. Numerical calculations indicate that, to a good approximation, $C_{wg}' \sim 4e^2/\pi\hbar v_F$ except very near turn-on.

We therefore make the approximation $C_{wg}' \sim 4e^2/\pi\hbar v_F$, which should be an upper bound for the true capacitance when only one subband is occupied. We can then infer the mobilities of the tubes under electrolyte gating; for the data

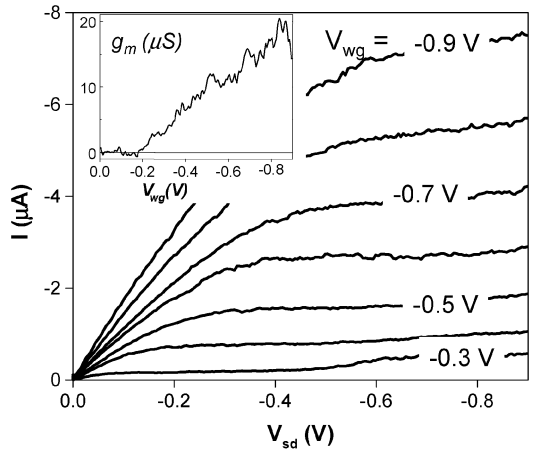

Figure 5. $I-V_{sd}$ characteristics of the device shown in Figure 2b at different water gate voltages ranging from −0.9 V to −0.3 V in 0.1 V steps (top to bottom). The inset shows the transconductance $g_m = dI/dV_{wg}$ taken at $V_{sd} = -0.8$ V.

in Figure 2a, this gives $\mu \sim 1000$ cm^2/V−s. This is in good agreement with the mobility obtained for the same device in vacuum, $\mu = 1500$ cm^2/V−s. This agreement implies that (a) the mobility of the tube is not dramatically affected by the electrolyte, and (b) the elecrolyte tube capacitance is near the quantum capacitance. These measurements illustrate that water-gated nanotube FETs approach the ultimate limit where the capacitance is governed by quantum effects and not electrostatics.

We now discuss the nonlinear transport performance characteristics of water-gated nanotubes. Figure 5 shows $I-V$ curves at different V_{wg} values in the p-region. The current initially rises linearly with V_{sd} and then becomes constant in the saturation region. The transconductance in the saturation region, $g_m = dI/dV_{wg}$, grows approximately linearly with $|V_{wg} - V_{wgo}|$, as shown in the inset, reaching a value of 20 μA/V. Measurements on other samples give comparable results. This transconductance is approximately 1 order of magnitude larger than the highest values previously reported for SWNT transistors.[3,6]

The large g_m follows directly from the high mobility and large gate capacitance found above. From standard FET analysis, $g_m = C_g'|V_g - V_{go}|\mu/L$. Using the linear response measurements above, this equation predicts a g_m of 27 μA/V at an overvoltage of 0.7 V, in reasonable agreement with the measured value. Normalizing the transconductance to the device width of ∼3 nm gives $g_m/W \sim 7$ μS/nm. This is an order of magnitude greater than the transconductance per unit width for current-generation MOSFETs.

The results above show that nanotubes have very high transconductances. The ultimate limit would be a ballistic nanotube transistor with a gate capacitance given by C_Q': $g_m = 4e^2/h = 150$ μA/V. The transistors reported here are within a factor of 5−10 of this limit. Since the devices we have studied to date are still quite long (1 μm), a reduction of the channel length to ∼200 nm should approach the ballistic limit, assuming that the contacts can be made ideal. Experiments in our group are currently underway to achieve this limit. The excellent device characteristics of SWNT transistors in salty water also indicate that they may be ideal for biosensing applications. Since a SWNT has dimensions comparable to typical biomolecules (e.g., DNA, whose width is approximately 2 nm), they should be capable of electrical sensing of single biomolecules. A charged molecule near the SWNT will act as an effective gate, changing the conductance of the tube. The large transconductances reported above indicate that the signal from single molecules should be readily observable.

Acknowledgment. This work was supported by the NSF Center for Nanoscale Systems, the Packard Foundation, and the MARCO Focused Research Center on Materials, Structures, and Devices, which is funded at the Massachusetts Institute of Technology, in part by MARCO under contract 2001-MT-887 and DARPA under grant MDA972-01-1-0035. Sample fabrication was performed at the Cornell node of the National Nanofabrication Users Network, funded by NSF.

References

(1) Martel, R.; Schmidt, T.; Shea, H. R.; Hertel, T.; Avouris, Ph. *Appl. Phys. Lett.* **1998**, *73*, 2447−9.
(2) McEuen, P. L.; Bockrath, M.; Cobden, D. H.; Yoon, Y.-G.; Louie, S. G. *Phys. Rev. Lett.* **1999**, *83*, 5098.
(3) Zhou, C. W.; Kong, J.; Dai, H. J. *Appl. Phys. Lett.* **2000**, *76*, 1597−1599.
(4) Bachtold, A.; Hadley, P.; Nakanishi, T.; Dekker, C. *Science* **2001**, *294*, 1317−1320.
(5) Javey, A.; Shim, M.; Dai, H. *Appl. Phys. Lett.* **2002**, *80*, 1064.
(6) Wind, S. J.; Appenzeller, J.; Martel, R.; Derycke, V.; Avouris, Ph. *Appl. Phys. Lett.* **2002**, *80*, 3817−3819.
(7) Tans, S. J.; Verschueren, R. M.; Dekker, C. *Nature* **1998**, *393*, 49−52.
(8) Kong, J.; Franklin, N. R.; Zhou, C.; Chapline, M. G.; Peng, S.; Cho, K.; Dai, H. *Science* **2000**, *287*, 622.
(9) Cui, Y.; Wei, Q.; Park, H.; Lieber, C. M. *Science* **2001**, *293*, 1289−92.
(10) Kong, J.; Soh, H. T.; Cassell, A.; Quate, C. F.; Dai, H. *Nature* **1998**, *395*, 878.
(11) Krüger, M.; Buitelaar, M. R.; Nussbaumer, T.; Schönenberger, C.; Forró, L. *Appl. Phys. Lett.* **2001**, *78*, 1291−3.
(12) Wildoer, J. W. G.; Venema, L. C.; Rinzler, A. G.; Smalley, R. E.; Dekker, C. *Nature* **1998**, *391*, 59−62.
(13) Park, J.; McEuen, P. L. *Appl. Phys. Lett.* **2001**, *79*, 1363−5.
(14) Bockrath, M.; Hone, J.; Zettl, A.; McEuen, P. L.; Rinzler, A. G.; Smalley, R. E. *Phys. Rev. B* **2000**, *61*, R10606−8.
(15) Lee, R. S.; Kim, H. J.; Fischer, J. E.; Lefebvre, J.; Radosavljevic, M.; Hone, J.; Johnson, A. T. *Phys. Rev. B* **2000**, *61*, 4526−9.
(16) Zhou, C.; Kong, J.; Yenilmez, E.; Dai, H. *Science* **2000**, *290*, 1552−5.
(17) Martel, R.; Derycke, V.; Lavoie, C.; Appenzeller, J.; Chan, K. K.; Tersoff, J.; Avouris, Ph. *Phys. Rev. Lett.* **2001**, *87*, 256805.
(18) Tans, S. J.; Devoret, M. H.; Dai, H.; Thess, A.; Smalley, R. E.; Georliga, L. J.; Dekker, C. *Nature* **1997**, *386*, 474−7.
(19) Bockrath, M.; Cobden, D. H.; McEuen, P. L.; Chopra, N. G.; Zettl, A.; Thess, A.; Smalley, R. E. *Science* **1997**, *275*, 1922−5.
(20) Cobden, D. H.; Bockrath, M.; McEuen, P. L.; Rinzler, A. G.; Smalley, R. E. *Phys. Rev. Lett.* **1998**, *81*, 681−4.
(21) Shim, M.; Javey, A.; Kam, N.; Dai, H. *J. Am. Chem. Soc.* **2001**, *123*, 11512−11513.
(22) Fuhrer, M. S.; Kim, B. M.; Dürkop, T.; Brintlinger, T. *Nano Lett.* **2002**, *2*, 755.

NL025639A